Journal of Environmental Chemical Engineering 10 (2022) 107977

Contents lists available at ScienceDirect

Journal of Environmental Chemical Engineering

journal homepage: www.elsevier.com/locate/jece

Tailoring the permeability and flux stability of forward osmosis membrane with tert-butylamine functionalized carbon nanotubes for paracetamol removal

Wei Jie Lee, Pei Sean Goh *, Woei Jye Lau, Kar Chun Wong, Nur Diyana Suzaimi, Ahmad Fauzi Ismail

Advanced Membrane Technology Research Centre, Faculty of Chemical and Energy Engineering, Universiti Teknologi Malaysia, 81310 Johor, Malaysia

ARTICLE INFO

Editor: Despo Kassinos

Keywords:
Amino-functionalized carbon nanotubes
Thin film nanocomposite membrane
Paracetamol removal
Forward osmosis

ABSTRACT

The discharge of pharmaceutical wastewater is an adversity to the nature. Some of the pharmaceutical product (PP) wastes are highly resistant towards bio-degradation hence physical-based separation technology such as forward osmosis (FO) has been introduced for the treatment. Despite exhibiting high water flux, commercial FO membrane often suffers from fouling and unsatisfactory solute rejection. In this study, carbon nanotubes (CNT) which has high self-bundling tendency was functionalized with tert-butylamine (TBA), a bulky tertiary amine. The agglomeration of the aminated CNT was suppressed via steric hindrance and surface charge repulsion. The nanofillers was then incorporated into the polyamide (PA) layer of thin film nanocomposite (TFN) during interfacial polymerization process to provide the required hydrophilicity and surface charges. Using synthetic paracetamol (PCT) solution as the feed solution (FS), the experimental outcome showed that the incorporation of amino-functionalized CNT (ACNT) successfully enhanced the hydrophilicity and flux stability of the FO membranes. Compared to the control thin film composite (TFC) membrane, ACNT-TFN membrane exhibited an improved water flux from 3.58 $L.m^{-2}.h^{-1}$ to 9.01 $L.m^{-2}.h^{-1}$, without sacrificing the PCT rejection (99.7 %). This study improves the understanding on the superior benefits of FO for enhancing the pharmaceutical waste removal and stimulates insight for more nanofillers-induced modification on the FO membrane, in order to make it truly useful for more water separation applications in the future.

1. Introduction

In recent years, the global consumption of pharmaceutical products (PPs) is on rise due the increasing consumption of pharmaceutical products (PPs) in many daily activities. The disposal of PPs to water stream is a potential source of environmental pollution. Due to their constant presence in drinking water, surface water, ground water and urban water, the living organism and environment can be adversely affected [1]. The PPs in wastewater may ultimately end up in drinking water at trace concentration from 0.1 ng L^{-1} to 1 μg L^{-1} [2,3]. Many types of PPs, such as paracetamol (PCT), ciprofloxacin, and isoniazid are strongly resistant towards biological degradation and can deposit for a long period [4]. The disposal of PPs into wastewater leads to chronic effects such as bio-accumulation that is hazardous towards terrestrial and aquatic organisms. For instance, it can induce resistance development in pathogenic microbes, genotoxicity, aquatic toxicity, and endocrine disruption [5]. Therefore, PPs are recognized as a concerned anthropogenic pollutants [6–9]. Studies have been extensively conducted to determine the exact concentration of trace PPs in aquatic environment. The concentration of PPs detected in aquatic environment is up to parts per trillion, or ng. L^{-1}, primarily sourced from veterinary and human usage [10,11].

Among the PPs, the most used drugs world-wide are analgesic and antipyretic drugs. These drugs can be commonly used to treat multiple prevalent diseases and can be bought over the counter without medical prescription [12]. One of the most popularly used analgesic and antipyretic drugs is PCT, or acetaminophen, as it can be easily obtained and the consumption procedure is simple. PCT is chosen as the subject of this study in view of its prevalence among the analgesia family and common existence in natural and drinking water [13,14]. Furthermore, compared to the other drugs of analgesia family, PCT has the highest concentration in aquatic environment [15–19]. Processes like flocculation, advanced

* Corresponding author.
E-mail addresses: weijie934@hotmail.com (W.J. Lee), peisean@petroleum.utm.my (P.S. Goh).

https://doi.org/10.1016/j.jece.2022.107977
Received 12 March 2022; Received in revised form 21 May 2022; Accepted 23 May 2022
Available online 26 May 2022

oxidation process (AOP) and adsorption are less favorable in this green-era due to shortcomings like high energy consumption, low efficiency and potential secondary pollution [20]. Hence, the urge to identify the more suitable PCT removal method arises in recent years.

Membrane technology, crowned as the 'water treatment technology in 21st century', has been widely exploited in the area of seawater desalination, food and pharmaceutical production, and environmental protection [21–23]. Membrane processes can be easily categorized by its pore size, from one to thousands of nanometer, namely microfiltration (MF), ultrafiltration (UF), nanofiltration (NF), and reverse osmosis (RO) [24–26]. With different pore sizes, the process can be easily modified to cater for the removal of different suspended and dissolved solids, which is promising for actual industrial wastewater treatment. Due to the small solute size of PCT, MF and UF are not effective in removing PCT up to a disposable level [26], while NF and RO are effective in removing PCT from stream [27–29]. Despite the efficiency of removing PPs from streams of impaired quality, these processes require high pressure hence is not favorable for the overall operational cost. The pressure-driven processes are highly-susceptible to membrane fouling thus periodical cleaning as well as large membrane area are essential to ensure a stable production [30,31]. The necessary periodical membrane further imposes additional expenses. Thus, alternative membrane processes with low fouling propensity and high energy-effectiveness is highly desired.

Forward osmosis (FO) is a feasible alternative to these pressure-driven processes. It applies the same rejection mechanisms, but with a less frequent fouling propensity and nearly zero energy consumption, winning itself an important seat in the field of water treatment [32–34]. Instead of applying pressure, FO utilizes osmotic pressure gradient as the driving force to induce flow of pure water from a low osmotic pressure FS to a high osmotic pressure draw solution (DS) across a semi-permeable membrane [35]. In comparison to the conventional water treatment methods, FO is recognized as a potential candidate for the removal of PPs, and creates insight for more renowned alternatives that are environmental-friendly, highly energy-efficient and cost-effective. For instance, Jang et al. [25] treated 12 types of emerging PPs including PCT using FO. The results showed a promising solute rejection of greater than 80 % for all the PPs.

To fully exploit the advantages of FO, the internal concentration polarization (ICP) issue, which often associated to its water flux, must be addressed[36,37]. To tackle this issue, Hou et al. [38] incorporated carbon nanotubes (CNTs) onto the membrane surface layer. Due to the water channel and superior hydrophilicity rendered by CNTs, the water flux has been significantly improved. The selectivity of the resultant membrane was also improved due to the narrow and precise aperture of CNTs. However, one major challenge confronted by this innovative thin film nanocomposite (TFN) membrane is the poor compatibility between the CNT and the polymer matrix. Due to the high aspect ratio and twisted configuration, CNTs agglomerate easily [39]. This can be a major setback as the overall transport performance of the membrane depends critically on the membrane nanoscale interface morphology [40,41]. Ideally, homogeneous nanofillers dispersion is favorable for defect-free TFN membrane fabrication especially when the nanofillers are incorporated into the ultrathin selective layer of TFN. In this study, amino functionalization was adopted to overcome this challenge. Amino functional groups were introduced on the CNTs surface to act as a barrier to reduce the inter-tube Van de Waals force of attraction between CNTs molecules and sterically hinders entanglement of CNTs. Interfacial polymerization (IP) was carried out to form polyamide (PA) selective layer atop substrate layer, while tert-butylamine (TBA) was added during the reaction. The use of TBA is considered as a novel approach for CNT functionalization and TFN membrane fabrication. It is convinced that its relative bulkiness of TBA to other nanofillers or amine is perfect to induce steric hindrance which suits the purpose of this study. Three parameters were studied, i.e. water flux, solute rejection and performance stability. The amino functionalization also serves the purpose of tweaking the polarity of CNTs to further enhance the rejection and flux stability of the resultant TFN membranes.

2. Experimental

2.1. Materials

Multi-walled CNTs (MWCNTs) (outer diameter × inner diameter × length: 10 nm × 4.5 nm × 4.5 μm) were purchased from Sigma Aldrich. HNO_3 (75 %) and H_2SO_4 (99.5 %) used to pre-treat the CNTs before amino-functionalization were purchased from Sigma Aldrich. Tert-butylamine (98 %, Sigma-Aldrich) was used for functionalization of CNTs. Ethanol (≥95 %, EAM) was used for post-washing of CNTs. Polysulfone (PSF UDEL P3500) used for substrate fabrication was obtained from Solvay. Polyvinylpyrrolidone (PVP, K30, Sigma-Aldrich) was used as pore-former whereas N-methyl pyrrolidone (NMP, ≥98.5 %, EAM) was used as solvent to dissolve PSF. TMC (98 %, fisher scientific) in n-hexane (95 %, Merck) and m-phenyldiamine (MPD) (98 %, Merck) in RO water (Milli-Q Direct 8) were used in IP to form PA layer. NaCl (99.5 %, Merck) was used as DS, while PCT (98 %, $C_8H_9NO_2$, 151.163 g.mol^{-1}, pKa 9.38, Sigma Aldrich) was used as FS. 2000 ppm of PCT stock solution was prepared by dissolving 2.0 g of PCT dried solid in 10 mL of ethanol, and further mixed with deionized (DI) water until 1.0 L mark at pH 7. The mixture was then stirred using a mechanical stirrer until all PCT was completely dissolved.

2.2. Synthesis of amino-functionalized carbon nanotubes

The pristine MWCNTs were refluxed in a mixture of 5 M H_2SO_4 and 5 M HNO_3 with volume ratio 3:1 at 90 °C for 24 h to obtain oxidized carbon nanotube (OCNT). The OCNTs were washed with DI water to neutralize its pH to 7. To produce ACNT, 100 mL of TBA and 1 g of MWCNTs were stirred at room temperature for 24 h. The black suspension formed was washed with ethanol for several times. The resultant ACNTs were dried overnight in oven at 70 °C and ground into fine powder. To avoid adsorption of moisture, the ACNT powder was sealed tightly in a glass vial and stored inside a desiccator.

2.3. Preparation of membranes

Phase inversion technique was employed to prepare the TFC and TFN substrate. The components used for substrate dope comprised of 17 wt% of PSF, 82.0 wt% of NMP, and 1.0 wt% of PVP. Firstly, PVP was introduced into the NMP solvent. After that, the dope was mechanically stirred at 200 rpm and 60 °C until all PVP was fully dissociated to form a homogeneous solution. Then, PES pellets were gently added into the dope followed with mechanical stirring for another 24 h until the pellets were completely dissolved. To remove the trapped air bubbles, the dope was left at room temperature for another 24 h. Furthermore, the substrate was cast by pouring the dope on a glass plate and rolled swiftly, then instantly immersed into a pure water bath for around 3 min. Finally, the solidified substrate was removed from the glass plate and soaked in DI water overnight to remove the remaining solvent.

The PA layers was formed via IP [42]. The substrate produced was placed on a clean and dried glass plate. A rubber roller was then employed to remove excess water droplet on its surface because it could not mix evenly with the inorganic solvent, which would in turn interrupt the PA layer formation. After that, the substrate was confined on a glass frame using paper clips. The monomers concentration used in both organic and aqueous solutions were TMC/n-hexane [w/v: 0.1 (g/100 mL)] and MPD/H_2O [w/v: 2.0 (g/100 mL)], respectively. Firstly, 30 mL of aqueous solution was poured onto the substrate surface and left untouched for 5 min to ensure sufficient penetration of the MPD monomers into the support layer pores. The solution was then poured off and the water droplets on membrane surface were rolled off using rubber roller. Next, 40 mL of TMC organic solution was poured on the substrate surface and left untouched for 1 min to ensure successful formation of PA

layer. The TMC organic solution was poured off and allowed for air-drying at room temperature. Finally, the membrane was post-treated in an oven at 60° C for 8 min. The pristine TFC membrane was stored in DI water until further usage. The ACNTs incorporated TFN membrane was prepared using the same procedure, except that ACNTs (0.1 mg. mL^{-1} – 0.5 mg.mL^{-1}) were pre-dispersed in aqueous solution via 1 h of sonification prior to PA layer formation. Fig. 1 depicts the preparation processes of nanofiller and membrane.

2.4. Characterization of nanofillers and membranes

Raman spectrometer (inVia™, Renishaw) was used to measure the intensity ratio of D-band and G-band (I_d/I_g) to indicate the disorder degree of graphitic structure of CNTs. D-band represents the degree of defects while G-band represents the degree of graphitization. Argon ion laser beam (λ_{Raman} = 514 nm) was used to irradiate the powdered samples powder and the process was controlled below 30 s for each scanning to prevent sample degraded by the laser beam. Fourier-transform infrared spectroscopy (FTIR, Frontier, Perkin Elmer) was used to confirm the introduction of carboxylic acid and amide groups. The chemical compounds on the nanofillers were identified by detecting the characteristic bands of functional groups and specific bonds via infrared spectroscopy. Infrared spectrum of the modified nanofillers were compared with the pristine nanofillers highlight and identify the odd infrared absorption bands. The powdered membrane samples were molded into cylindrical KBr pellets and analysis was done on the surface. Spectrum was recorded between 600 cm^{-1} and 4000 cm^{-1}.

Field emission scanning electron microscopy (FESEM, S4800, Hitachi) was used to characterize the surface and cross-sectional morphologies of PSF substrate, TFC and TFN membranes. Morphological studies provide information about the structure of membranes which can be correlated with the membrane performance and to determine possible defect formation. The thickness of the skin layer was also identified. Meanwhile, the topological and chemical profiles of membranes were identified using atomic force microscopy (AFM, 5200 S, Hitachi) and FTIR accordingly. Surface roughness and topology are important features that determine the permeation flux of the membranes.

Water contact angle measurement was done by using contact angle system OCA (708381-T, LMS Scientific). The movement of water across the membrane was observed, and the contact angle measurement and water movement were used to identify the hydrophilicity of the membrane surface. Besides, zeta potential, ζ of membrane surfaces and PCT at different pH were measured using zeta potential analyzer (ELSZ-1000, Otsuka).

2.5. Forward osmosis performance evaluation

The cross-flow FO cell with an effective membrane area of 20.02 cm^2 was used for the separation performance testing. Throughout the FO process, the system was operated at 300 rpm to circulate the FS and DS using two variable speed pumps. AL-DS and AL-FS modes were both carried out. The temperatures of FS and DS were fixed at ambient temperature. 2000 ppm synthetic PCT solution was employed as FS while 2.0 M NaCl solution was employed as DS. To obtain a precise water flux, the DS tank was placed on a digital weight balance to record the weight change of DS each 30 min Fig. 2 shows the complete setup for the lab-scale FO system.

The water flux, J_v ($L.m^{-2}.h^{-1}$) was calculated by applying Eq. (1):

$$Jv = \frac{\Delta V}{A \quad \Delta t} \tag{1}$$

where ΔV is the volume change of the FS (mL), A is the effective area of membrane (0.002002 m^2) Δt is the operating time interval (h). Meanwhile, the reverse salt flux (RSF, $g.m^{-2}.h^{-1}$) was calculated using Eq. 2 based on the change in salt concentration and FS volume:

$$Js = \frac{\Delta C_f \Delta V}{A \quad \Delta t \times 1000} \tag{2}$$

where ΔV (mL) and ΔC_f ($g.L^{-1}$) are the change in volume of FS from beginning till the end of a time interval and salt concentration change in FS accordingly. The conductivity of FS was obtained using a conductivity meter probe, then further plotted into concentration curve to create a calibration graph.

Besides, the PCT rejection (R_{PCT}) was calculated using Eq. 3 by measuring the difference of the initial concentration of PCT in FS and the final of concentration of PCT in DS for every 30 min using high-performance liquid chromatography (HPLC).

$$RPCT = 1 - [(\frac{C_{f,DS}}{C_{i,FS}}) \times 100] \quad \% \tag{3}$$

where $C_{f,DS}$ and $C_{i,FS}$ represents the final concentration and initial concentration of PCT in DS and FS respectively. The flux stability assessment is carried out on the TFC and TFN membrane under AL-FS mode for 6 h.

3. Results and discussions

3.1. Characteristics of synthesized nanofillers

The ATR-FTIR spectra of pristine CNTs, OCNTs, and ACNTs are shown in Fig. 3(a). The spectra data of CNTs was observed and two characteristics peaks were distributed in the range of 3300–2500 cm^{-1} and 2100–2400 cm^{-1}. Two broad peaks were observed at 2115 cm^{-1} and 2335 cm^{-1} in all CNTs, which represent the C-H bending of aromatic carbon compounds. Meanwhile, the oxidation of CNTs using acids pair formed OCNTs. COOH groups were introduced and confirmed by noticing the broad peak in the range of 3300–2500 cm^{-1}, centered at 3000 cm^{-1}. It indicates O-H stretching of the hydroxyl group from carboxyl groups (C-OH and O═C-OH), which is less distinctive in ACNTs as some of the hydroxyl groups were substituted by amine forming amide groups [43]. However, in pristine CNTs, the peaks that represent carboxyl groups was also observed at 2600 cm^{-1}. Its existence suggested that partial oxidation had occurred during purification process by the manufacturer [43]. Similar observation was found in the negative shift at 1366 cm^{-1} which represents O-H bending of COOH functional group, whereby ACNTs had a dimmer peak due to amide substitution. Strong bond of C═O stretching, however could be found almost equally sharp in both OCNTs and ACNTs at 1740 cm^{-1}, implying that the carbonyl groups were retained throughout the amino functionalization. The introduction of tertiary amine forming ACNTs could be further verified by observing the negative shift at 1214 cm^{-1}, indicating C-N stretching of amide III. However, it is important to know that tertiary amine does not contain N-H stretching like primary and secondary amines due to the fully engaged alkyl groups.

As calculated from the Raman spectra shown in Fig. 3(b), the l_D/l_G ratio of CNT increased from 0.95 to 0.98 after acid treatment, indicating that the graphitic order of nanotubes was slightly disrupted upon oxidation, as SP_2 bonds were being transformed into SP_3 bonds. Besides, the intercalation of the oxygenated groups such as carboxyl and hydroxyl groups has induced inter-repulsion, resulting in an increased l_D. Meanwhile, compared to the oxidized counterparts, ACNT had a mere higher l_D/l_G ratio due to a relatively smaller sp^2 in-plane vibration of carbon atoms that results in lower l_G value [44]. The deposition of TBA potentially occupied the remaining space of sp^2 domain and further restricted the vibration. In other words, it can also be explained that the deposition of TBA has imposed minor defects on the graphitic structure.

3.2. Characteristics of modified membranes

Fig. 4 depicts the ATR-FTIR spectra of the membranes. Apart from

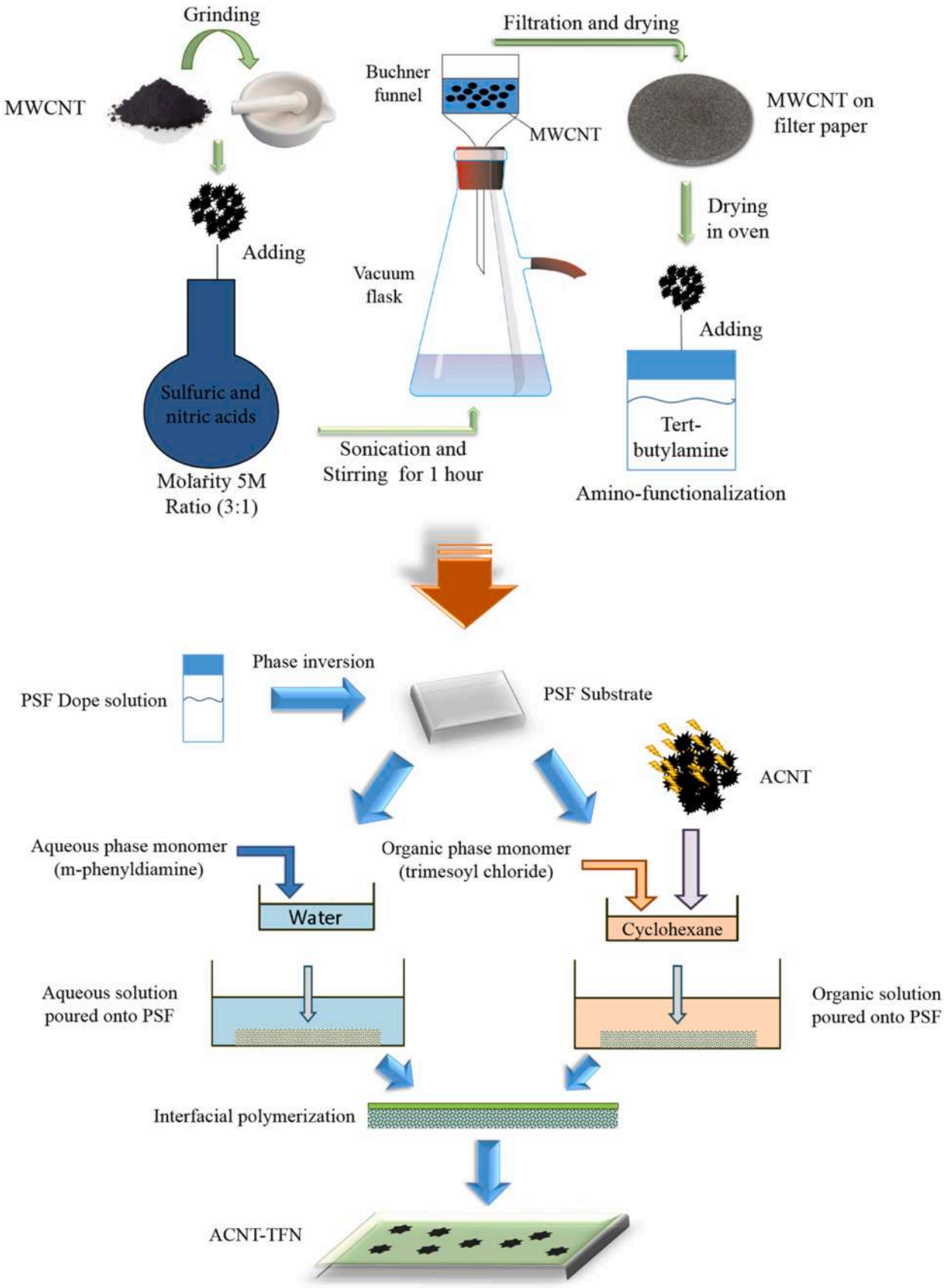

Fig. 1. Schematic diagram of nanofiller and membrane preparation.

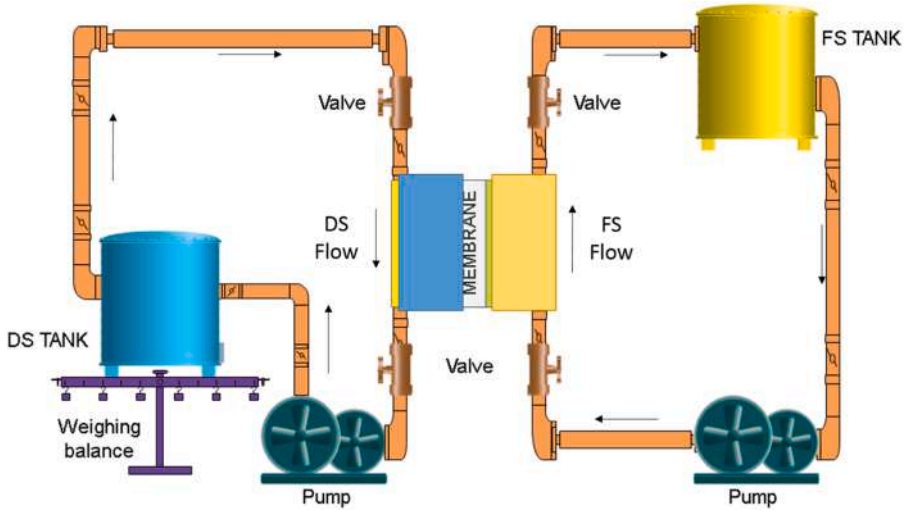

Fig. 2. Schematic diagram of bench-scale forward osmosis setup used in this study.

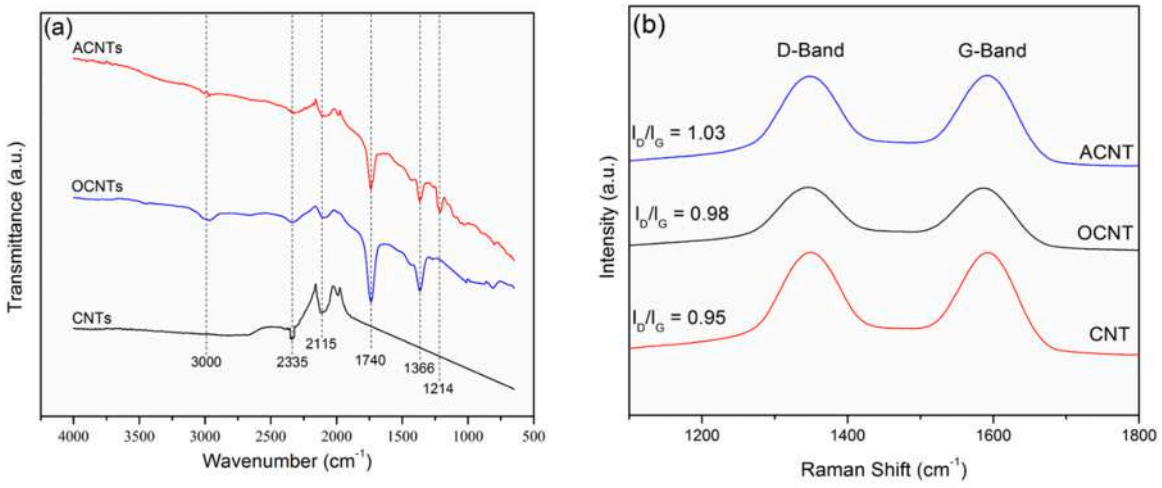

Fig. 3. (a) ATR-FTIR and (b) Raman spectra of pristine and modified CNTS.

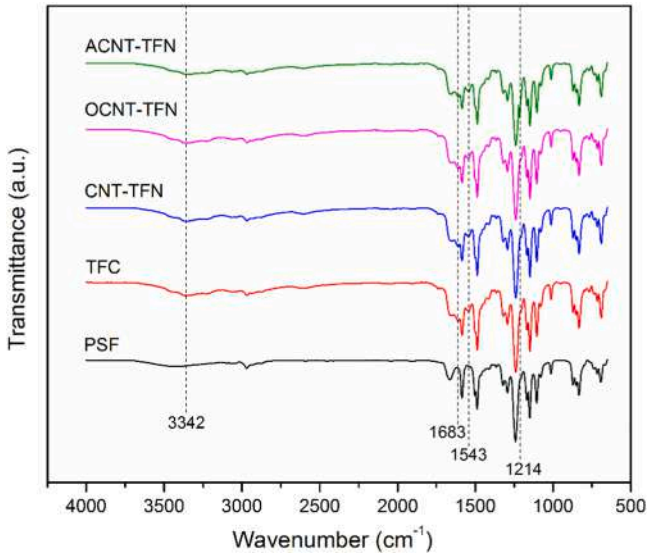

Fig. 4. ATR-FTIR spectra of membranes.

PSF substrate, distinctive peaks at 3342 cm^{-1}, 1683 cm^{-1} and 1543 cm^{-1} which correspond to amine II (N-H stretching), amide I (C═O stretching) and amide II (N-H bending), respectively were detected in all the TFC and TFN membranes. The detection of element N as the main component of PA layer has confirmed the successful formation of PA layer atop PES support. Meanwhile, for ACNT-TFN membrane, it could be noticed that the presence of peak at 1214 cm^{-1} which represents amide III (C-N stretch from tertiary amide) and successful incorporation of ACNT. Apparently in OCNT-TFN membrane, the peak of amide III is absent. Meanwhile, all the remaining peaks for the functional groups of CNT derivatives could still be seen in the IR spectra of composite membranes, indicating that the C-H bonds were not disrupted during the PA layer deposition process.

Highly-crosslinked selective PA layer was deposited on the PSF support surface via IP of two immiscible monomers, namely TMC in organic solution and MPD in aqueous solution. Initially, ACNTs were pre-experimentally added to both aqueous and organic phase during IP process, which was then further found out that the latter method yield more uniform structure. This could be attributed by n-hexane as the solvent in organic phase required no physical removal as it would evaporate in atmospheric condition, but water as the solvent in aqueous phase was removed by rolling and air-drying which further interfered the orientation of ACNTs on membrane surface. Compared to the surface

of PSF support layer, PA layer is much rougher, as evident from the AFM images shown in Fig. 5. At the same time, the incorporation of nanofillers could further increase the surface roughness significantly, as coarser nodular structure would form upon encapsulation of the rigid nanofillers within the growing PA layer, in turn creating higher ridges [45]. The root mean square surface roughness (R_q) of the membranes was obtained from their height profile images. It could be contradictorily noticed that the surface roughness of ACNT-TFN (R_q =52.86 nm) was nearly on-par with TFC (R_q =45.51 nm), indicating the incorporation of ACNT did not cause subdued uniformity. In fact, ACNT was also proven to be highly absorptive towards membrane, hence it could be perfectly embedded in the PA layer without creating ridges on the surface [46]. On the other hand, the CNT-TFN and OCNT-TFN membranes had the surface roughness almost double of their counterparts due to the uneven distribution of nanofillers. The thickness of PA layer also significantly increased with the incorporation of nanofillers, whereby the average thickness was around 100 nm and 200 nm for TFC and TFN membranes, respectively. Wong et al. [46] reported an increase membrane thickness by 100 nm upon the incorporation of CNTs in the TFN membranes.

The surface morphology of the membranes is depicted in Fig. 6. It could be clearly noticed that the surfaces of all TFC and TFN membranes were covered with leaf-like structures arranged in the form of ridge-valley, a symbolic structure for PA layer. Besides, on the membrane surface, it could be observed that CNTs without functionalization clustered into an irregular shape (Fig. 6e). As CNTs are highly-dense and nano-sized compounds in long tubular shape, self-bundling is often inevitable. At first, sonication was carried out to ensure all the nanofiller suspensions were well-dispersed in the organic phase monomer solution. After that, pristine CNTs were oxidized using sulphuric acid/nitric acid pairs to potentially reduce the clustering phenomenon as carboxylic acid groups were introduced into CNT forming bulkier compound (Fig. 6g). By comparing CNT-TFN (Fig. 6e) with OCNT-TFN (Fig. 6g), the size of cluster has reduced significantly. The addition of ACNT was able to efficaciously solve the clustering phenomenon. The inter-nanotubular Van der Waals force of attraction was lowered through TBA deposition, and also due to the fact that TBA is a tertiary compound which prevents agglomeration by steric hindrance [47]. Hence, in Fig. 6, it was noticeable that the degree of agglomeration of CNT was greatly reduced after acids and TBA functionalization, in which ACNT-TFN (Fig. 6i) exhibited the most uniform nanofiller dispersion across the membrane surface. At 60x magnifications, Figs. 6f, h, and j provide a clearer view of the nanotubes entanglement. The pristine CNTs (Fig. 6f) were bundling among themselves on the membrane surface which created an extremely dense region followed by a relatively sparse region.

Fig. 7 depicts the cross-sectional morphology of PSF substrate and TFC/TFN membranes. It could be noticed that the deposition of PA layer did not significantly increase the thickness of membrane surfaces, instead, a relatively flat surface was featured. It implies the complete penetration of substrate pores by monomers and the resultant PA layers were firmly attached onto the substrate. All membranes exhibited long finger-like structure and highly porous middle part to ease the water diffusion and effectively reduce water transport resistance. The base consisted of dense modules followed by left-like structures extending to the upper part of the selective layer [48]. Such structure was induced by the interfacial degassing of CO_2 that are encapsulated between the support layer and the selective layer [49]. Generally, the membranes are comprised of two primary layers: (1) spongy highly-porous support layer; (2) microporous support membrane formed via phase inversion on top of non-woven support layer. For TFC/TFN membranes, there is another ultrathin active layer atop microporous support membrane accounted for solute rejection, which is absent in PSF support (Fig. 7a). Furthermore, the CNT cluster is highly visible from the cross-sectional image, while a rather smooth and uniform surface was observed on the ACNT incorporated TFN.

The membrane surface hydrophilicity is influenced by its surface chemical composition, topology and roughness. The water contact angle values of the membranes are compared in Fig. 8. The water contact angle of the TFN membrane embedded with ACNTs was much lower than that of neat TFC membrane. From the aspect of surface topology, CNTs which are tubular in structure could provide a good channel for water inflow. From the aspect of chemical composition, the functionalization of CNTs introduced abundant oxygen-rich functional groups that could impart surface hydrophilicity. Additionally, the modification of CNTs with TBA further granted hydrophilic amide functional groups to the CNTs, and reduced the water contact angle of membrane surface upon incorporation. According to the Cassie-Baxter model, the increased surface roughness also partly contributed to the enhanced surface hydrophilicity of the TFN membranes [50]. Hence, the membrane overall surface hydrophilicity was significantly enhanced, while the water contact angle was reduced from $69.33 \pm 2.24^{\circ}$ for TFC to $58.03 \pm 1.93^{\circ}$ for ACNT-TFN. Besides, the high standard deviation of CNT-TFN membrane strongly suggests that the clustering phenomenon has affected the overall consistency of membrane hydrophilicity at different points of contact. Ihsan et al. [45] who incorporated CNTs onto the membrane observed that the surface hydrophilicity of membranes has been

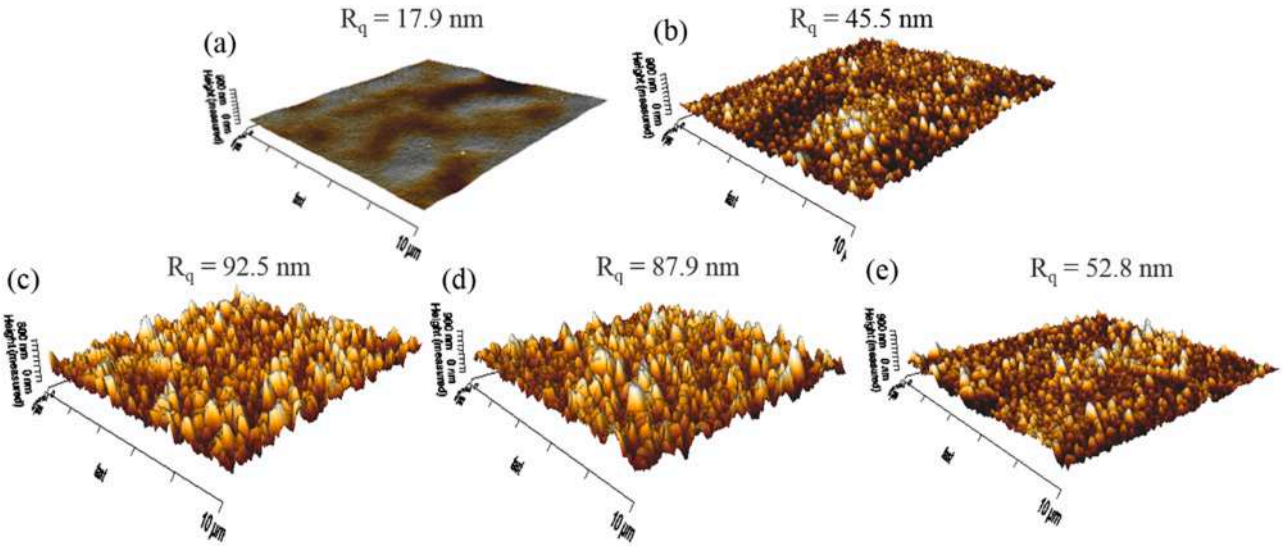

Fig. 5. Three dimensional AFM images of (a) PSF, (b) TFC, (c) CNT-TFN, (d) OCNT-TFN, and (e) ACNT-TFN with root mean square surface roughness, R_q labeled.

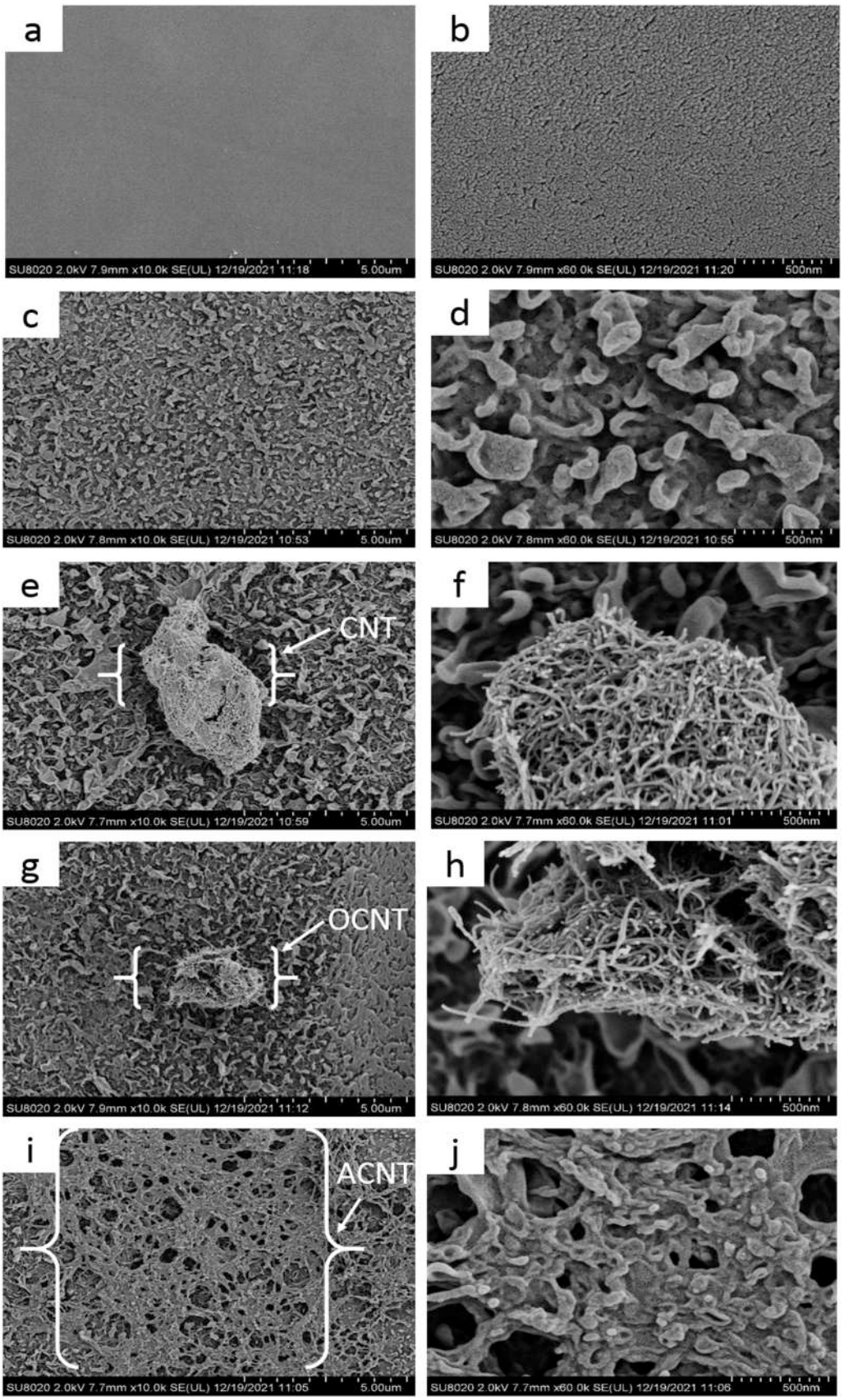

Fig. 6. FESEM images with magnification of x 10k (left column) and x 60k (right column), displaying surface morphology of (a, b) PSF, (c, d) TFC, (e, f) CNT-TFC, (g, h) OCNT-TFC, and (i, j) ACNT-TFC.

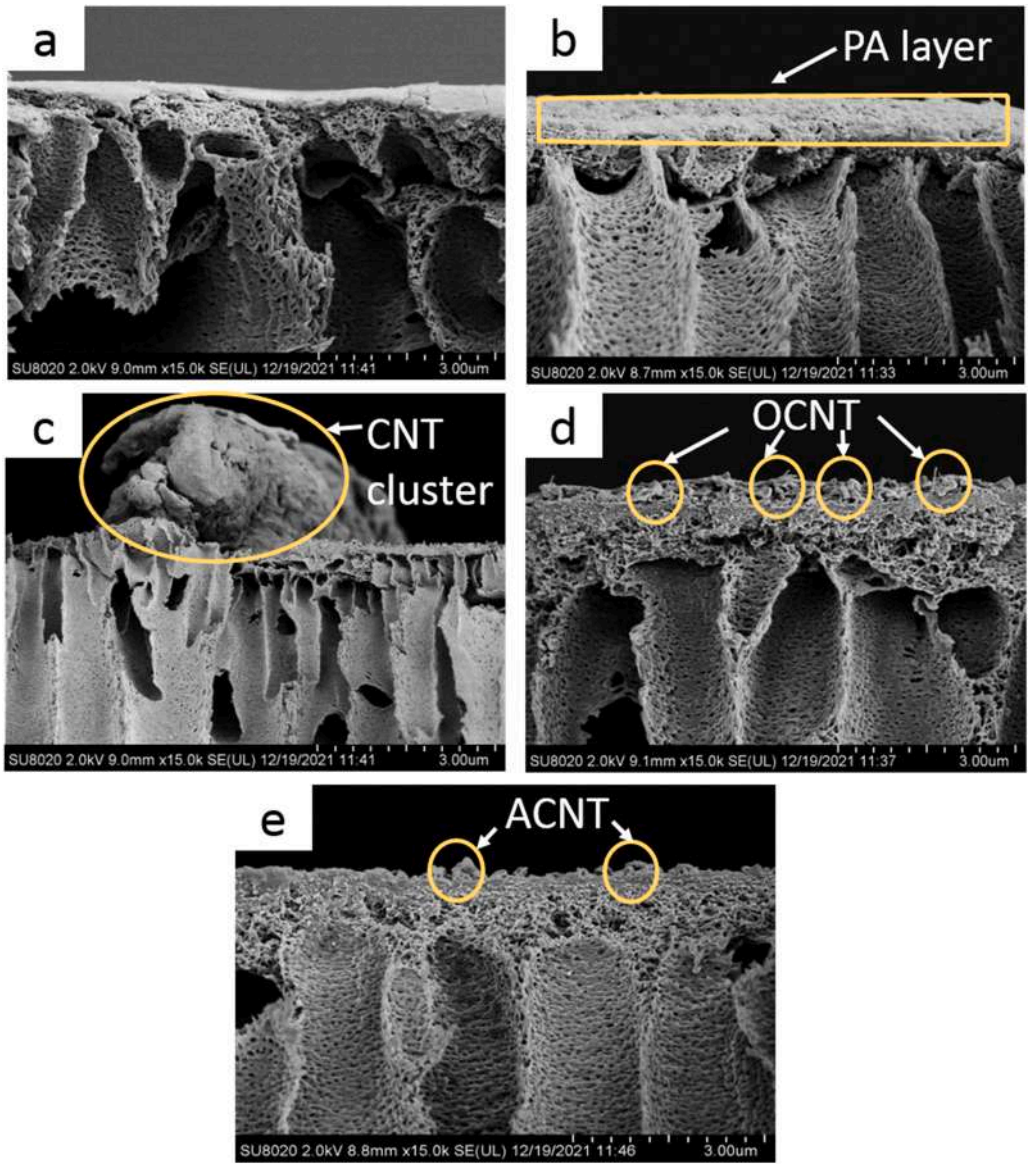

Fig. 7. FESEM cross-sectional images of (a) PSF, (b) TFC, (c) CNT-TFC, (d) OCNT-TFC, and (e) ACNT-TFC with magnification of x 15.

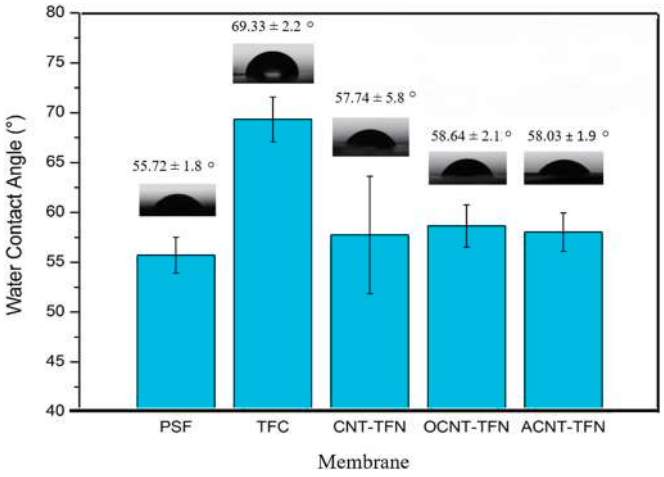

Fig. 8. Water contact angle of the TFC and TFN membranes.

significantly reduced due to the hydrophilic nature of the surface modified CNTs.

3.3. Performance evaluation

3.3.1. Water flux and reverse salt flux

The water flux and RSF are indicated in Fig. 9(a). The results suggested that the incorporation of CNT successfully imparted hydrophilicity to the membrane surfaces. Water flux improvement could be significantly observed on TFC membrane from 3.58 $L.m^{-2}.h^{-1}$ to 7.96 $L.m^{-2}.h^{-1}$ for OCNT-TFC and 9.01 $L.m^{-2}.h^{-1}$ for ACNT-TFC membranes. This improvement represented increment by around 100–150 %. The tubular structure of CNT provides extra channel to facilitate water transport at each instance. The flux improvement can be ascribed to the increasing surface hydrophilicity and surface roughness as witnessed from the previous characterization results. Meanwhile, the CNT-TFC membrane had an average water flux of 21.04 $L.m^{-2}.h^{-1}$, granting it the highest water flux among all. Nonetheless, high water flux alone does not ensure an efficacious performance, as RSF, the measurement of the backflow of salt solutes from DS to FS, is also another important indicator to judge the membrane overall performance. A high RSF

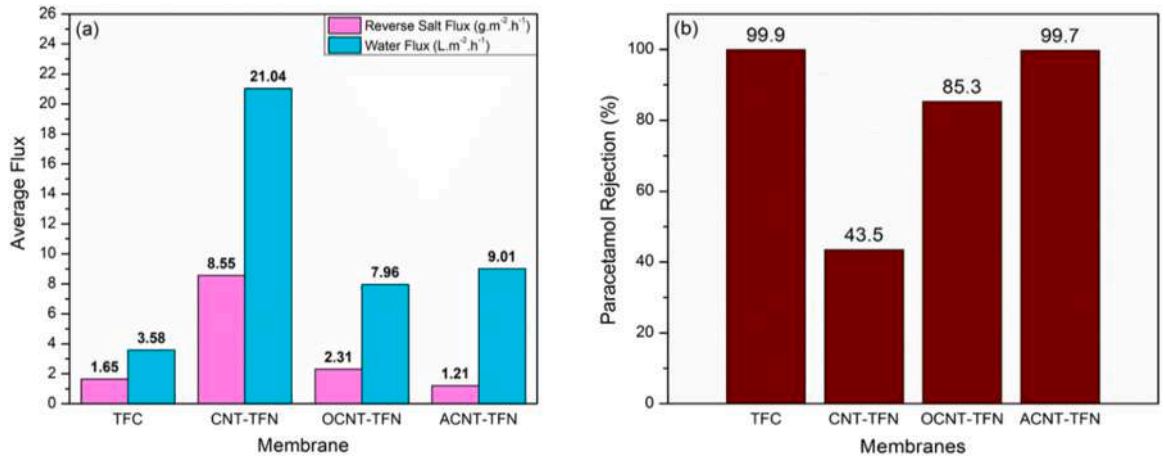

Fig. 9. The performances of TFC and TFN membranes in terms of (a) Average fluxes and (b) PCT rejection under AL-FS mode.

implies high salt selectivity, which is commonly observed in a defective membrane. Usually, a defective PA layer formation results in solute leakage that is highly undesired. It was observed that, despite having a higher water flux, the CNT-TFN membrane exhibited RSF that was prominently 4 – 8 folds higher than that of other membranes prepared in this study. An ideal ratio between water flux and RSF needs to be achieved. In addition, a high RSF tends to cause the dilution of draw solute over time, ensuing the loss of drawing power. Consequently, a prolonged process would eventually reach state of osmotic equilibrium whereby the net flow of water and solute becomes zero. ACNT-TFN exhibited the highest water to salt ratio of 7.44 compared to other membranes. The lower water flux and higher RSF of OCNT-TFN suggested that the minor entanglement of OCNT has resulted in the formation of defective membrane. Apparently, high water flux usually indicates high RSF, yet ACNT-TFN has out-performed TFC with a high water flux but low RSF. It can be deduced that during the osmotic process, the hydrophilic nanotube channels were engaged by water, hence reducing the tendency for salt diffusion. As evidenced from the FESEM images in Fig. 7, the CNT cluster is highly visible, which further correlates to the bad flux performance, as it could potentially block the pores of active layer or cause defective surface instead of acting as a water channel.

3.3.2. *Paracetamol rejection*

The modification of membranes should only be considered successful when the rejection ability of membrane is not sacrificed. For the TFC membrane prepared in this study, an almost complete PCT rejection of 99.9 % has been achieved, as depicted in Fig. 9(b). It is crucial to investigate the relationship and effects of CNT incorporation on PCT rejection, whether the rejection ability is compromised through the alteration of membrane surface structure. The findings depict that the PCT rejection on CNT-modified membranes increased in the order of functionalization degree from CNT-TFN, OCNT-TFN, to ACNT-TFN correspond to the value of 43.5 %, 85.3 %, and 99.7 % accordingly. This suggests that the rejection was not affected by the incorporation of CNT, yet poor distribution of the nanofillers could adversely affect the performance. By comparing the rejection performance to RSF, similarity was found. The fact is, while a hydrophilic membrane should be favorable towards high water selectivity, high RSF indicates high solute selectivity regardless of feed or draw solutes. It implies that solutes are transfusable on both sides of the membranes, and hence RSF is commonly said to be another indicator for solute rejection performance. It usually implies a defective membrane. The rejection study also reflects that the degree of defectiveness is inversely proportional to the degree of functionalization, with more uniform nanofiller functionalization yields better rejection.

The schematic diagram presented in Fig. 10 illustrates the mechanisms of water transport and rejection of pristine and modified membranes. A summary of recent FO studies on PCT rejection is tabulated in Table 1. Due to the difference in the parameters evaluated in each study, selectivity has been used as the benchmark to evaluate water

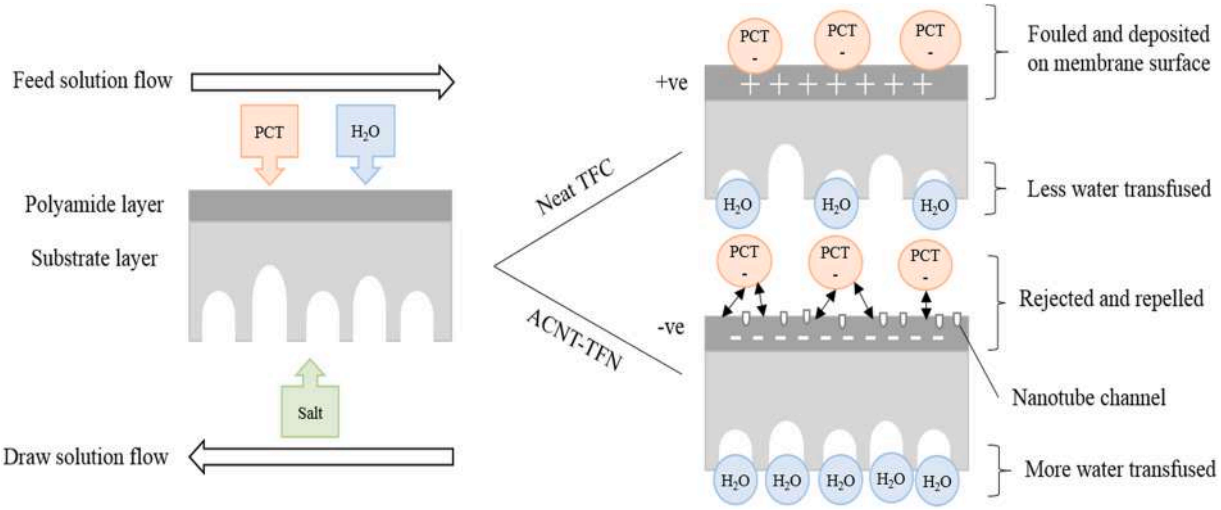

Fig. 10. Schematic illustration of water transport and solute rejection for TFC and TFN membranes.

Table 1
Comparative study of FO on pharmaceutical wastewater rejection.

Membrane	Feed solution	Draw solution	Water flux (L. $m^{-2}.h^{-1}$)	Reverse salt flux (g. $m^{-2}.h^{-1}$)	Water selectivity	Rejection (%)	Ref.
*Biomimetic aquaporin hollow fiber	Emerging contaminants (including PCT)	0.25–2 M NaCl	8.58	1.24	6.92	96.2	[52]
*Commercial FO TFC	Emerging contaminants (including PCT)	0.5 M NaCl	22.4	18.58	1.21	80.1	[25]
Commercial FO TFC	Trace organic contaminants (including PCT)	0.5 M NaCl	5.6	2.744	2.04	~90	[53]
ACNT-TFN	Synthetic PCT solution	2 M NaCl	9.01	1.21	7.44	99.7	Current Study

* The studies had several parameters yielding different data, hence average readings were obtained.

permeability of the membrane as it represents the ratio of water to salt diffusivity despite the parameter difference. The TFN membrane prepared in the present study exhibited the highest water selectivity of 7.44. Despite the impressive water flux, the membrane reported by Jang et al. has suffered from high RSF [25]. In term of rejection, the current study also possessed the higher rejection among all, indicating that the resultant membrane was defect-free. The commercial FO membrane has a lower rejection due to the adsorption mechanism of emerging contaminants, whereby hydrophilic contaminants like PCT has a lower mass adsorption than hydrophobic contaminants on membrane surface. The considerable concentration of hydrophobic emerging contaminants causes accumulated adsorption on commercial FO membrane surface, consequently allowing more compounds to permeate through the membrane, hence the rejection is lower [51].

3.3.3. *Flux stability assessment*

Flux drop is an inevitable issue in membrane separation as the available pores are accumulated with solutes. The incorporation of ACNT was proven to be a viable approach to resolve the issue. The water flux trend shown in Fig. 11 shows that ACNT-TFN demonstrated a steady water flux of ~9 $L.m^{-2}.h^{-1}$ throughout the filtration, while the TFC membrane was suffering flux recession from 4.28 $L.m^{-2}.h^{-1}$ to 2.79 $L.m^{-2}.h^{-1}$. The flux drop of TFC membrane was steeper at the early stage of the process, and subsequently became steady until the end of experiment, implying that the water-solute transfusion on membrane pore has reached equilibrium state. Meanwhile, CNT-TFN exhibited inconsistent water flux, correlated to high standard deviation from water contact angle analysis. The flux decline issue was mainly alleviated by charge repulsion. The data from literature states that industrial pharmaceutical wastewater containing PCT has a pH range of 7 – 9 [54,55]. In this study, the PCT was prepared in DI water of pH 7. The correlation between pH and charges was investigated through zeta potential analysis. The information regarding the point zero charge pH (pH_{ZPC}) of the adsorbent which is membrane surface and pKa of the adsorbate which is paracetamol is crucial to investigate the effect of pH on the adsorption mechanism. From Fig. 12, it could be observed that the pH_{ZPC} of TFC was at 9.2, while for ACNT-TFN was not found within this pH range. The change in pH of the process affects the process dynamics and adsorption chemistry [56]. The membrane surface becomes positively-charged when pH < pH_{ZPC}, and negatively-charged when pH > pH_{ZPC}. Meanwhile, as PCT is a substituted phenol with pKa of 9.38, the adsorption of substituted phenol depends on the solution pH. At acidic pH, PCT remains un-dissociated and dispersed, while at neutral to basic pH, PCT dissociates and converts into anion. As the process was operated at pH 7, PCT was in anionic form and hence adsorption occurred due to electrostatic attraction between PCT anion and positively-charged TFC surface. In the meantime, the ACNT incorporation has tweaked the surface of TFN towards negatively-charged, due to the presense of ionized carboxylic acid and amide groups. The electrostatic repulsion from negative charges prevented adsorption uptake, in turn assuring consistent water flux. Uniform dispersion of ACNT across the membrane surface and low surface roughness suggest a low tendency of potential solute accumulation. However, as this study only focused on PCT solution, the limitation is that the flux decline could be more severe during the treatment of real wastewater which consists of metals and salts as fouling could occur due to the interference of organic and inorganic materials. In the future study, experimental work will be conducted to evaluate the long-term fouling performance using real-time foulants.

4. Conclusion

In a nutshell, CNT was acid-treated followed by amino-

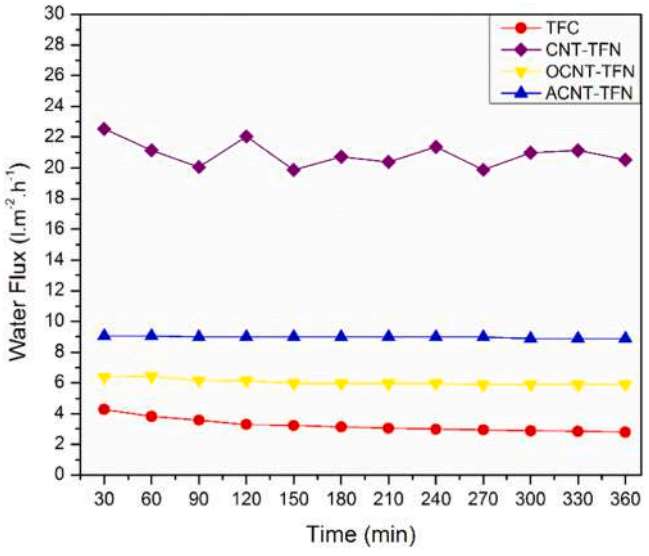

Fig. 11. Water flux distribution curve over 360 min.

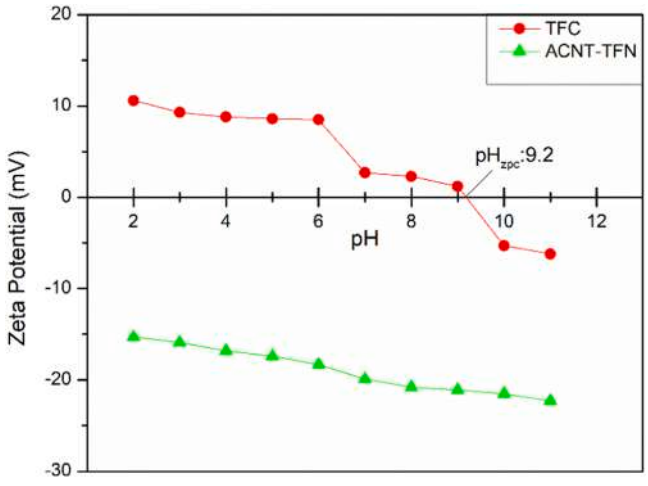

Fig. 12. Zeta potential of PCT and membranes at different pH.

functionalization and incorporated onto PA layer of TFN membranes. The effects of ACNT incorporation were studied through two means, which are characterization using different instruments and FO performance study employing PCT solution as FS. During the IP process, desired interaction happened between nanofillers and monomers, forming a defect-free active layer of superior hydrophilicity. It was demonstrated that the CNT suffered from entanglement issue which tends to form bulky CNT clusters. TBA serves as a good dispersant to prevent the agglomeration of CNT in aqueous solution. The nanofillers characteristics such as zeta potential and hydrophilicity successfully altered the properties of the PA layer into a more favorable one. Consequently, the ACNT-TFN membrane exhibited a significantly improved surface hydrophilicity and flux stability with a water flux of 9.01 $L.m^{-2}.h^{-1}$ which could be consistently maintained throughout 360 min, without sacrificing the salt rejection at 99.7 %. Some physical characteristics were also altered upon nanofiller incorporation, such as increase in thickness from 100 nm to 200 nm, and surface roughness from 45.51 nm to 52.86 nm. However, the effects on membrane performance were not significant. It is hoped that this study could provide the understanding of the effects of membrane modification and nanofiller incorporation towards the improvement of FO process. It also contributes to the future development of TFN membrane and grants insight on the potential of this FO membrane for the removal of other emerging contaminants or PPs.

CRediT authorship contribution statement

Wei Jie Lee: Conceptualization, Methodology, data preparation, writing and draft preparation. **Pei Sean Goh:** Supervision, writing, reviewing. **Woei Jye Lau:** Supervision, reviewing. **Kar Chun Wong:** Methodology, idea discussion. **Nur Diyana Suzaimi:** Methodology, sample preparation. **Ahmad Fauzi Ismail:** Reviewing.

Declaration of Competing Interest

The authors declare that they have no known competing financial interests or personal relationships that could have appeared to influence the work reported in this paper.

Acknowledgements

The authors gratefully acknowledge financial support given by the Malaysian Ministry of Higher Education under HiCOE Grant 4J435.

References

[1] D. Kanakaraju, B.D. Glass, M. Oelgemöller, Advanced oxidation process-mediated removal of pharmaceuticals from water: a review, J. Environ. Manag. 219 (2018) 189–207.
[2] L. Sellaoui, et al., Adsorption of amoxicillin and paracetamol on modified activated carbons: equilibrium and positional entropy studies, J. Mol. Liq. 234 (2017) 375–381.
[3] J.L. Zhou, et al., Pharmaceutical residues in wastewater treatment works effluents and their impact on receiving river water, J. Hazard. Mater. 166 (2) (2009) 655–661.
[4] J. Nyirenda, A. Mwanza, C. Lengwe, Assessing the biodegradability of common pharmaceutical products (PPs) on the Zambian market, Heliyon 6 (10) (2020), e05286.
[5] V. Rakić, et al., The adsorption of salicylic acid, acetylsalicylic acid and atenolol from aqueous solutions onto natural zeolites and clays: clinoptilolite, bentonite and kaolin, Microporous Mesoporous Mater. 166 (2013) 185–194.
[6] P.I. Ali, V. Gupta, Advances in water treatment by adsorption technology, Nat Protoc. 1 (2006) 2661–2667.
[7] W.S. Adriano, et al., Adsorption of amoxicillin on chitosan beads: kinetics, equilibrium and validation of finite bath models, Biochem. Eng. J. 27 (2) (2005) 132–137.
[8] A.M. Redding, et al., A QSAR-like analysis of the adsorption of endocrine disrupting compounds, pharmaceuticals, and personal care products on modified activated carbons, Water Res. 43 (2009) 3849–3861.
[9] L.A. Al-Khateeb, S. Almotiry, M.A. Salam, Adsorption of pharmaceutical pollutants onto graphene nanoplatelets, Chem. Eng. J. 248 (2014) 191–199.
[10] S.D. Richardson, T.A. Ternes, Water analysis: emerging contaminants and current issues, Anal. Chem. 90 (1) (2018) 398–428.
[11] A. Sangion, P. Gramatica, Hazard of pharmaceuticals for aquatic environment: prioritization by structural approaches and prediction of ecotoxicity, Environ. Int. 95 (2016) 131–143.
[12] Y. Valcárcel, et al., Analysis of the presence of cardiovascular and analgesic/anti-inflammatory/antipyretic pharmaceuticals in river- and drinking-water of the Madrid Region in Spain, Chemosphere 82 (7) (2011) 1062–1071.
[13] Ali, P.I., Chiral Pollutants: Distribution, Toxicity and Analysis by Chromatography and Capillary Electrophoresis. 2004.
[14] W. Edrees, et al., A review on comparative study between the physicochemical and biological processes for paracetamol degradation, Univers. J. Pharm. Res. 2 (2017) 18–29.
[15] A. Kwarciak-Kozłowska, 7 - Removal of pharmaceuticals and personal care products by ozonation, advance oxidation processes, and membrane separation, in: M.N.V. Prasad, M. Vithanage, A. Kapley (Eds.), Pharmaceuticals and Personal Care Products: Waste Management and Treatment Technology, Butterworth-Heinemann, 2019, pp. 151–171.
[16] G. Dai, et al., Occurrence and source apportionment of pharmaceuticals and personal care products in the Beiyun River of Beijing, China, Chemosphere 119 (2015) 1033–1039.
[17] C. Ávila, J. García, Chapter 6 - pharmaceuticals and personal care products (ppcps) in the environment and their removal from wastewater through constructed wetlands, in: E.Y. Zeng (Ed.), Comprehensive Analytical Chemistry, Elsevier, 2015, pp. 195–244.
[18] N. Nakada, et al., Pharmaceutical chemicals and endocrine disrupters in municipal wastewater in Tokyo and their removal during activated sludge treatment, Water Res. 40 (17) (2006) 3297–3303.
[19] Y. Yang, et al., Occurrences and removal of pharmaceuticals and personal care products (PPCPs) in drinking water and water/sewage treatment plants: A review, Sci. Total Environ. 596–597 (2017) 303–320.
[20] J. Gao, et al., Superwetting PVDF membrane prepared by in situ extraction of metal ions for highly efficient oil/water mixture and emulsion separation, Sep. Purif. Technol. 275 (2021), 119174.
[21] Q. Cheng, et al., Facile fabrication of superhydrophilic membranes consisted of fibrous tunicate cellulose nanocrystals for highly efficient oil/water separation, J. Membr. Sci. 525 (2017) 1–8.
[22] X. Zhao, et al., Engineering superwetting membranes through polyphenol-polycation-metal complexation for high-efficient oil/water separation: from polyphenol to tailored nanostructures, J. Membr. Sci. 630 (2021), 119310.
[23] J. Zhu, et al., Microporous organic polymer-based membranes for ultrafast molecular separations, Prog. Polym. Sci. 110 (2020), 101308.
[24] K.P.M. Licona, et al., Assessing potential of nanofiltration and reverse osmosis for removal of toxic pharmaceuticals from water, J. Water Process Eng. 25 (2018) 195–204.
[25] D. Jang, et al., Relating solute properties of contaminants of emerging concern and their rejection by forward osmosis membrane, Sci. Total Environ. 639 (2018) 673–678.
[26] J. Garcia-Ivars, et al., Rejection of trace pharmaceutically active compounds present in municipal wastewaters using ceramic fine ultrafiltration membranes: effect of feed solution pH and fouling phenomena, Sep. Purif. Technol. 175 (2017) 58–71.
[27] L.D. Nghiem, A.I. Schäfer, M. Elimelech, Pharmaceutical retention mechanisms by nanofiltration membranes, Environ. Sci. Technol. 39 (19) (2005) 7698–7705.
[28] A.I. Schäfer, L.D. Nghiem, T.D. Waite, Removal of the natural hormone estrone from aqueous solutions using nanofiltration and reverse osmosis, Environ. Sci. Technol. 37 (1) (2003) 182–188.
[29] X. Jin, J. Hu, S.L. Ong, Removal of natural hormone estrone from secondary effluents using nanofiltration and reverse osmosis, Water Res. 44 (2) (2010) 638–648.
[30] K.L. Hickenbottom, et al., Forward osmosis treatment of drilling mud and fracturing wastewater from oil and gas operations, Desalination 312 (2013) 60–66.
[31] P.H.H. Duong, et al., Highly permeable double-skinned forward osmosis membranes for anti-fouling in the emulsified oil-water separation process, Environ. Sci. Technol. 48 (8) (2014) 4537–4545.
[32] B. Mi, M. Elimelech, Organic fouling of forward osmosis membranes: fouling reversibility and cleaning without chemical reagents, J. Membr. Sci. 348 (1–2) (2010) 337–345.
[33] C.R. Martinetti, A.E. Childress, T.Y. Cath, High recovery of concentrated RO brines using forward osmosis and membrane distillation, J. Membr. Sci. 331 (1) (2009) 31–39.
[34] X. Song, et al., Fabrication of carbon nanotubes incorporated double-skinned thin film nanocomposite membranes for enhanced separation performance and antifouling capability in forward osmosis process, Desalination 369 (2015) 1–9.
[35] T.Y. Cath, A.E. Childress, M. Elimelech, Forward osmosis: principles, applications, and recent developments, J. Membr. Sci. 281 (1) (2006) 70–87.
[36] H.-Q. Liang, et al., Forward osmosis membranes with unprecedented water flux, J. Membr. Sci. 529 (2017) 47–54.
[37] J.R. McCutcheon, M. Elimelech, Influence of concentrative and dilutive internal concentration polarization on flux behavior in forward osmosis, J. Membr. Sci. 284 (1) (2006) 237–247.
[38] Hou, Y., et al., Hydrophilic carbon nanotube membrane enhanced interfacial evaporation for desalination, Chin. Chem. Lett., 2021.
[39] J. Pan, L. Bian, A physics investigation for influence of carbon nanotube agglomeration on thermal properties of composites, Mater. Chem. Phys. 236 (2019), 121777.

[40] M.E. Kojabad, et al., A novel high-performance facilitated transport membrane by simultaneously using semi-mobile and fixed carriers for CO_2/N2 separation, Process Saf. Environ. Prot. 156 (2021) 304–314.
[41] B. Wang, et al., High-performance membrane with angstrom-scale manipulation of gas transport channels via polymeric decorated MOF cavities, J. Membr. Sci. 625 (2021), 119175.
[42] W.J. Lee, et al., Antifouling zwitterion embedded forward osmosis thin film composite membrane for highly concentrated oily wastewater treatment, Sep. Purif. Technol. 214 (2019) 40–50.
[43] R. Sukor, et al., Modification strategy of screen-printed carbon electrode with functionalized multi-walled carbon nanotube and chitosan matrix for biosensor development, Asian J. Chem. 29 (2017) 31–36.
[44] D.B. Schuepfer, et al., Assessing the structural properties of graphitic and non-graphitic carbons by Raman spectroscopy, Carbon 161 (2020) 359–372.
[45] I. Wan Azelee, et al., Enhanced desalination of polyamide thin film nanocomposite incorporated with acid treated multiwalled carbon nanotube-titania nanotube hybrid, Desalination 409 (2017) 163–170.
[46] K.C. Wong, et al., The role of geometrically different carbon-based fillers on the formation and gas separation performance of nanocomposite membranes, Carbon 149 (2019) 33–44.
[47] W.J. Shaw, et al., Controls of nature: Secondary, tertiary, and quaternary structure of the enamel protein amelogenin in solution and on hydroxyapatite, J. Struct. Biol. 212 (3) (2020), 107630.
[48] S.C. Mamah, et al., Flux enhancement in reverse osmosis membranes induced by synergistic effect of incorporated palygorskite/chitin hybrid nanomaterial, J. Environ. Chem. Eng. 9 (4) (2021), 105432.
[49] W.-x Li, et al., Polyamide reverse osmosis membranes containing 1D nanochannels for enhanced water purification, J. Membr. Sci. 618 (2021), 118681.
[50] Y.J. Lim, et al., Unraveling the role of support membrane chemistry and pore properties on the formation of thin-film composite polyamide membranes, J. Membr. Sci. 640 (2021), 119805.
[51] J. Heo, et al., Comparison of flux behavior and synthetic organic compound removal by forward osmosis and reverse osmosis membranes, J. Membr. Sci. 443 (2013) 69–82.
[52] M. Salamanca, et al., Study of the rejection of contaminants of emerging concern by a biomimetic aquaporin hollow fiber forward osmosis membrane, J. Water Process Eng. 40 (2021), 101914.
[53] G. Blandin, et al., Impact of hydraulic pressure on membrane deformation and trace organic contaminants rejection in pressure assisted osmosis (PAO), Process Saf. Environ. Prot. 102 (2016) 316–327.
[54] M.E. Fawzy, et al., Sustainable approach for pharmaceutical wastewater treatment and reuse: case study, J. Environ. Sci. Technol. 11 (2018) 209–219.
[55] R.S. Rana, et al., A review on characterization and bioremediation of pharmaceutical industries' wastewater: an Indian perspective, Appl. Water Sci. 7 (1) (2017) 1–12.
[56] S.L. Wong, et al., Aspirin adsorption onto activated carbon derived from spent tea leaves: statistical optimization and regeneration study, Int. J. Environ. Res. 15 (2) (2021) 413–426.